analytical chemistry

ACS AuthorChoice

Article

pubs.acs.org/ac

Terms of Use

Identification of Virulence Determinants in Influenza Viruses

Pierre Negri,[†] Joo Young Choi,[†] Cheryl Jones,[‡] S. Mark Tompkins,[‡] Ralph A. Tripp,[‡] and Richard A. Dluhy*[,†]

[†]Department of Chemistry, University of Georgia, Athens, Georgia 30602 United States

[‡]Department of Infectious Disease, University of Georgia, Athens, Georgia 30602 United States

Supporting Information

ABSTRACT: To date there is no rapid method to screen for highly pathogenic avian influenza strains that may be indicators of future pandemics. We report here the first development of an oligonucleotide-based spectroscopic assay to rapidly and sensitively detect a N66S mutation in the gene coding for the PB1-F2 protein associated with increased virulence in highly pathogenic pandemic influenza viruses. 5′-Thiolated ssDNA oligonucleotides were employed as probes to capture RNA isolated from six influenza viruses, three having N66S mutations, two without the N66S mutation, and one deletion mutant not encoding the PB1-F2 protein. Hybridization was detected without amplification or labeling using the intrinsic surfaced-enhanced Raman spectrum of the DNA-RNA complex. Multivariate analysis identified target RNA binding from noncomplementary sequences with 100% sensitivity, 100% selectivity, and 100% correct classification in the test data set. These results establish that optical-based diagnostic methods are able to directly identify diagnostic indicators of virulence linked to highly pathogenic pandemic influenza viruses without amplification or labeling.

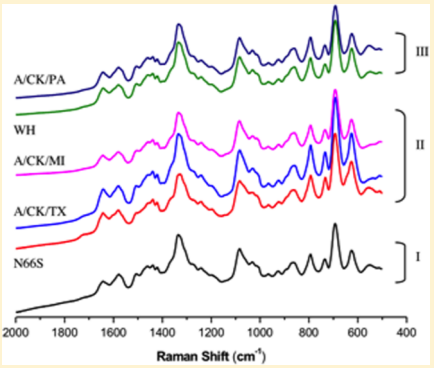

Influenza A virus is a ubiquitous negative strand RNA virus having pandemic potential.[1,2] Numerous studies have suggested that specific mutations in the HA, PB1, and NA genes are related to influenza virulence and pandemic potential.[3−6] The PB1-F2 protein has especially been linked to virulence since it is considered proapoptotic and pathogenic.[7−10] A N66S mutation in the PB1-F2 sequence is consistent among pathogenic influenza viruses, including the pandemic 1918 H1N1 and 1997 H5N1 highly pathogenic avian influenza strains, and is considered a virulence determinant.[11] Research shows that the N66S mutation correlates with significantly increased pathogenicity and mortality in mice and that PB1-F2 promotes secondary bacterial infections; the mechanism of increased virulence may be related to inhibition of interferon induction.[12] A recent global database analysis of the PB1-F2 protein revealed that the N66S mutation was present in only 3.8% of the H5N1 strains; however, the mutation was specifically found associated with the highly pathogenic strains.[13] In particular, all six H5N1 human isolates having the N66S mutation in the PB1-F2 protein isolated from Hong Kong influenza outbreaks were found to be highly pathogenic.[13] Given these data, it is apparent that the N66S mutation is relevant and critical for determining the pathogenic potential of influenza.

Development of a rapid and sensitive method for identifying emerging influenza viruses and determinants of virulence or pandemic potential is critical for control of transmission and disease intervention strategies. Currently, only genomic techniques such as PCR are available for laboratory diagnosis of virulence markers.[14,15] While these techniques provide identification of prognostic indicators, they rely entirely on genomic sequencing and alignment and can be limited by issues of reliability, standardization, and cost. Some studies of a commercial PCR test for influenza showed a relatively low sensitivity (∼75%);[16] the authors suggest the use of a more sensitive reference test to confirm negative results. The inability to provide definitive screening highlights the need for a diagnostic platform with high sensitivity, specificity, and expediency.

Our research groups have previously shown that surface-enhanced Raman spectroscopy (SERS) is a highly sensitive and specific method for direct, label-free detection of DNA-RNA binding.[17−22] The intrinsic Raman spectra of oligonucleotide probe-target complexes have been shown to be spectrally unique and sensitive to the hybridization of both matched and mismatched target sequences.[23−29] We recently reported on a SERS-based assay for identification of virulence factors associated with pathogenesis in influenza in model systems.[30] The current work shows that oligonucleotide-modified Ag nanorod arrays can be used for rapid and sensitive detection of pathogenicity determinants isolated from highly pathogenic and pandemic influenza viruses through direct identification of RNA and genetic mutations in PB1-F2 without amplification or labeling of the virus. The findings reported here provide the

Received: February 17, 2014
Accepted: June 17, 2014
Published: June 17, 2014

   dx.doi.org/10.1021/ac500659f | *Anal. Chem.* 2014, 86, 6911−6917

basis for oligonucleotide-based SERS screening of influenza with pandemic potential in a point-of-care application.

EXPERIMENTAL METHODS

Reagents. 6-Mercapto-1-hexanol (MCH) was purchased from Sigma-Aldrich (St. Louis, MO). All other chemicals were of analytical grade and used without any further purification. The hybridization buffer was prepared by dissolving 20 mM Tris HCl, 15 mM NaCl, 4 mM KCl, 1 mM $MgCl_2$, and 1 mM $CaCl_2$ in molecular biology grade water at pH 7.3; it was stored at 4 °C when it is not in use. The buffer and working tools were DNase free.

Preparation of Ag Nanorod SERS Substrates. Oblique-angle vapor deposition (OAD) was used to produce aligned Ag nanorod substrates for SERS applications, according to previously published methods.[31,32] In brief, standard glass microscope slides were cleaned using piranha solution, rinsed several times with deionized water, and dried using N_2 before being placed into a custom-designed, high vacuum electron beam vapor deposition chamber. Uniform thin film layers of Ti (20 nm) layer and Ag (500 nm) were first deposited onto the glass substrate at rates of 2.0 and 3.0 Å/s, respectively. The substrates were then rotated to 86° relative to the incident vapor source, and Ag nanorods were deposited at a constant rate of 3.0 Å/s until a nominal thickness of 2000 nm, as determined by a quartz crystal microbalance in the deposition chamber. These vapor deposition conditions result in optimal high aspect ratio Ag nanorod SERS substrates with overall nanorod lengths of ∼900 nm, diameters of ∼80−90 nm, densities of ∼13 nanorods/μm^2, and a tilt angle of 71° with respect to the substrate normal.[32] Following nanofabrication, a patterned multiwell array was produced on the Ag nanorod substrate according to previously published procedures.[33]

DNA Probes. DNA probes were purchased from Integrated DNA Technologies (IDT, Coralville, IA). The 5′-C6 thiolated ssDNA probes were received lyophilized and dissolved in molecular biology grade water to a concentration of 1000 nM. DNA probes were designed for viruses having determinants of low and high virulence in the PB1-F2 RNA, as previously described.[30]

Influenza Viruses. Three wild type influenza viruses were used in in these studies: A/Mute Swan/MS451072/06 (H5N1), A/CK/TX/167280-04/02 (H5N3), and A/CK/PA/13609/93 (H5N2).[34] The first two of these wild type viruses are examples of strains containing the N66S mutation, while the third did not have the mutation. Three additional reverse genetics viruses were used in these studies. These were the WH, WH N66S, and WH ΔPB1-F2 strains. These three viruses are 7:1 reassortants of A/WSN/33 (H1N1) with the PB1 segment (segment 2) of A/Hong Kong/156/97 (H5N1) highly pathogenic avian influenza virus. Two of these reverse genetics viruses contained either the wild type, intact PB1-F2 protein (WH), or the PB1-F2 protein with the N66S mutation (WH N66S). The third of the reverse genetics viruses was a negative control in which the PB1-F2 protein was deleted by removal of the start codon and introduction of two stop codons within the PB1-F2 open reading frame (WH ΔPB1-F2).[11,35]

MDCK cells were used to propagate the WH influenza viruses and were maintained in Dulbecco's Modified Eagles Medium (DMEM; GIBSO BRL Laboratories, Grand Island, NY) with 5% heat-inactivated (56 °C) FBS (Hyclone Laboratories, Salt Lake City, UT). For virus production, MDCK cells were rinsed three times with PBS, overlaid with 5 mL of MEM + TPCK trypsin (1 μg/mL; Worthington Biochemical, Lakewood, NJ) + virus and grown for 3−5 days at 35 °C until ∼70% cells were released from the flask surface. Supernatants containing virus were collected, centrifuged to remove cellular debris, aliquoted, and stored at −80 °C until use. Virus titers were quantified by hemagglutination (HA), 50% tissue culture infectious dose ($TCID_{50}$), and plaque assays as previously described.[36] The virus stock titer and PFU in 0.2 mL final volume for each of the influenza viruses used in this study are summarized in Table S.1 in the Supporting Information.

Viral Influenza RNA Samples. Viral RNAs isolated from six strains of influenza were used. This include three examples of N66S mutations (WH N66S, A/Mute Swan/MS451072/06, A/CK/TX/167280-04/02), and two without the N66S mutation (WH, A/CK/PA/13609/93). An influenza deletion mutant not containing the PB1-F2 sequence was used as a negative control (WH ΔPB1-F2). A PureLink Viral RNA/DNA mini Kit (Invitrogen, Carlsbad, CA) was used to isolate influenza virus RNA. Viral RNA was extracted by mixing 200 μL of each strain with 25 μL of Proteinase K in 1.5 mL followed by addition of 200 μL of 1× PBS/0.5% BSA in a microcentrifuge tube. The resulting solution was mixed for 15 s and then the lysate was incubated at 56 °C for 15 min. Subsequently, 250 μL of 96−100% ethanol was added, and then the lysate was mixed for 15 s followed by the incubation for 5 min at room temperature. The lysate was transferred onto the Viral Spin Column and centrifuged at 5 000 rpm for 1 min. The flow-through was discarded and the spin column was placed in a new collection tube. The washing step was repeated one more time with 500 μL of the wash buffer. The collection tube was discarded and the spin column was transferred into a new collection tube and spun at 13 000 rpm for 1 min to dry the column. The column was placed into a new recovery tube, and 50 μL of sterile, RNase-free water was added to the top of the the column. The resulting solution was incubated for 1 min at room temperature. The column was then centrifuged at 13 000 rpm for 1 min to elute the viral nucleic acids. Virus RNA purity and concentration was quantified by UV−vis spectrometry (Thermo Fisher NanoDrop 1000, Wilmington, DE).

Immobilization of DNA Probes onto Ag Nanorod Arrays. 5′-Thiol single stranded DNA (ssDNA) oligonucleotide probes were immobilized on the Ag nanorod array surface to capture and detect RNA strains corresponding to the PB1-F2 gene mutation. Preparation of self-assembled monolayers (SAMs) of ssDNA probes on the Ag nanorod substrates followed previously published procedures.[20,22,30] Briefly, 20 μL of 1000 nM of the oligonucleotide solution was added to a patterned microwell and incubated overnight at room temperature. After the incubation, any unbound oligonucleotide solution was removed from the microwell by rinsing it three times with molecular biology grade water and blow dried with N_2. Then, 20 μL of 100 nM solution of the spacer molecule 6-mercapto-1-hexanol (MCH) was added to the microwell in order to minimize nonspecific binding of DNA/RNA molecules to the surface of Ag nanorod substrates and for the correct oligonucleotide conformation. The spacer molecule was incubated for 6 h at room temperature followed by the rinsing and drying steps. A volume of 20 μL of 20 ng/μL (∼5 nM) RNA solution diluted in the binding buffer was added to the oligonucleotide-functionalized Ag nanorod to accomplish the hybridization and incubated at 37 °C for 2 h under a humid environment to avoid dehydration. After the incubation, any

dx.doi.org/10.1021/ac500659f | Anal. Chem. 2014, 86, 6911−6917

nonspecifically adsorbed RNA molecules were removed by rinsing with the binding buffer with the final wash using molecular biology grade water. The rinsed substrate was then dried with a gentle stream of N_2.

Raman Spectroscopy. Raman spectra were collected using a confocal Raman microscope (InVia, Renishaw, Inc., Hoffman Estates, IL) equipped with a 785 nm diode laser as the excitation source. The sample was illuminated through a 20× (Leica, Germany) N.A. = 0.40 objective with a spot size of approximately 4.8 μm × 27.8 μm; laser power was ~0.42 mW as measured at the sample. Spectra were collected between 2000−500 cm^{-1} using a 30 s acquisition time. Spectra were acquired from five different spots in each individual microwell on the Ag nanorod substrate. Four microwells were used for each sample; therefore, 20 spectra were collected for each sample and used for further data analysis.

Data Analysis. Prior to multivariate analysis, the raw spectra were preprocessed using a first order Savitzky−Golay derivative filter (15-point, second order polynomial), normalized to unit vector length, and mean centered. These preprocessing methods removed any spectral variations caused by instrumental drift, nonuniformity between different microwells on the substrate, and environmental changes. Initial spectral quality was assessed using principal component analysis (PCA). Determination of spectral outliers was based on calculation of their PCA scores with their corresponding Hotelling T^2 and Q residuals values.[37] Out of more than 140 spectra used in this analysis, only one spectral outlier was found and eliminated prior to analysis.

Multivariate analysis for classification was performed using partial least-squares discriminate analysis (PLS-DA)[38] and support vector machine discriminate analysis (SVM-DA).[39,40] All data processing was performed with PLS Toolbox version 6.2 (Eigenvector Research Inc., Wenatchee, WA) in MATLAB R2012a (The Mathworks Inc., Natick, MA).

RESULTS

Six influenza strains were used in this study. Three of these influenza strains contained the N66S mutation, representative of the putative PB1-F2 mutation consistent with increased virulence; these were the WH N66S, A/Mute Swan/MS45107206, and A/CK/TX167280-04/02 strains. Two other viruses were used that did not contain the N66S mutation and were representative of low virulence; these were the WH and A/CK/PA/13609/93 strains. A negative control virus was included, WH ΔPB1-F2, that had the open reading frame for the PB1-F2 protein deleted. For simplicity, viruses containing the N66S determinant are referred to as "high virulence" while the viruses not containing the N66S determinant are referred to as "low virulence." In addition to these samples, spectra of the DNA probe alone were collected and used in the analyses.

SERS spectra are shown in Figure 1A,B for the high and low virulence strains, respectively; each spectrum is an average of 20 individual spectra and is presented without processing. Figure 1A presents SERS spectra of the high virulence DNA probe-spacer complex before hybridization (Figure 1A,I), DNA-probe hybridized with complementary high virulence viral RNA strains (Figure 1A,II), and the DNA-probe incubated with noncomplementary low virulence viral RNA strains (Figure 1A,III). Figure 1B shows SERS spectra of the low virulence DNA probe-spacer complex alone (Figure 1B,I), the spectra of DNA-probe incubated with the noncomplementary high

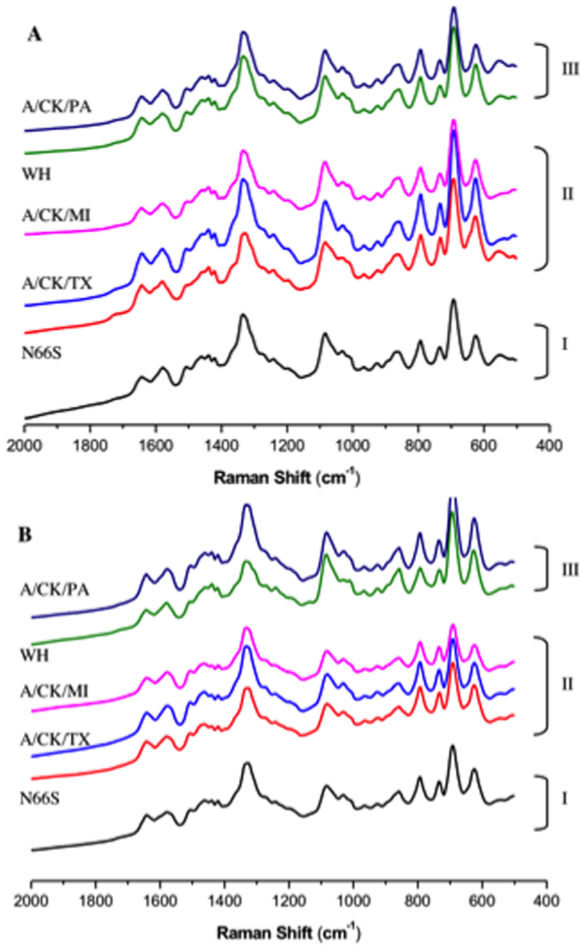

Figure 1. (A) Average SERS spectra of high virulence strains: (I) spectra of high virulence DNA probe, (II) spectra of high virulence DNA probe with complementary high virulence RNA strains (N66S, A/CK/TX, A/CK/MI), (III) spectra of DNA probe with noncomplementary low virulence RNA strains (WH, A/CK/PA). (B) Average SERS spectra of low virulence strains: (I) spectra of low virulence DNA probe, (II) spectra of LPAIV DNA probe with noncomplementary high virulence RNA strains (N66S, A/CK/TX, A/CK/MI), and (III) spectra of the low virulence DNA probe with complementary low virulence RNA strains (WH, A/CK/PA).

virulence viral RNA strains (Figure 1B,II), and DNA-probe incubated with the complementary low virulence viral RNA target sequence (Figure 1B,III). The dominant features found in the SERS spectra in Figure 1 correspond to nucleic acid vibrations, e.g., 1332, 1089, 1023, 793, and 623 cm^{-1}.[22,30]

The high virulence target RNA was distinguished from low virulence and control RNA using a whole-spectrum, multivariate statistical analysis of the Raman spectra. This method has been previously employed for detection, identification, and classification of pathogens.[41−43]

Partial least-squares discriminant analysis (PLS-DA) was utilized to build multivariate classification models to discern high virulence RNA binding to the substrate. The classification model was designed such that $^2/_3$ of spectra of the high virulence and low virulence RNA complexes were designated as a calibration/training sets, while the remaining $^1/_3$ of the spectra in each class were designated as the validation/prediction sets. This separation allowed the calibration model to contain all possible variances needed to explain the validation set. The spectra were randomly assigned to each

dx.doi.org/10.1021/ac500659f | Anal. Chem. 2014, 86, 6911−6917

set in order to minimize any correlation between spectral variances and order sequence. Cross-validation (Venetian blinds, 10 splits) was used for internal validation of the calibration model. The optimal number of latent variables (LVs) was selected based on the cross-validated class error.

Figure 2A,B represents the PLS-DA prediction results for the high virulence and low virulence assays, respectively, as a function of sample number. The prediction results for the samples in Figure 2 include both the calculated values for the calibration sets as well as the predicted values for the validation sets. Each icon in Figure 2 represents a SERS spectrum; the color code and shape of the symbol represents the particular class of samples the spectrum belongs to, as defined in the caption to Figure 2. The optimum threshold value for sample classification is represented by the red dashed line in Figure 2; the threshold is calculated using Bayes' Theorem based on the minimization of total classification errors.[44] Spectra with predicted values greater than the Bayesian threshold are designated as belonging to a particular category, as defined by the classification model.

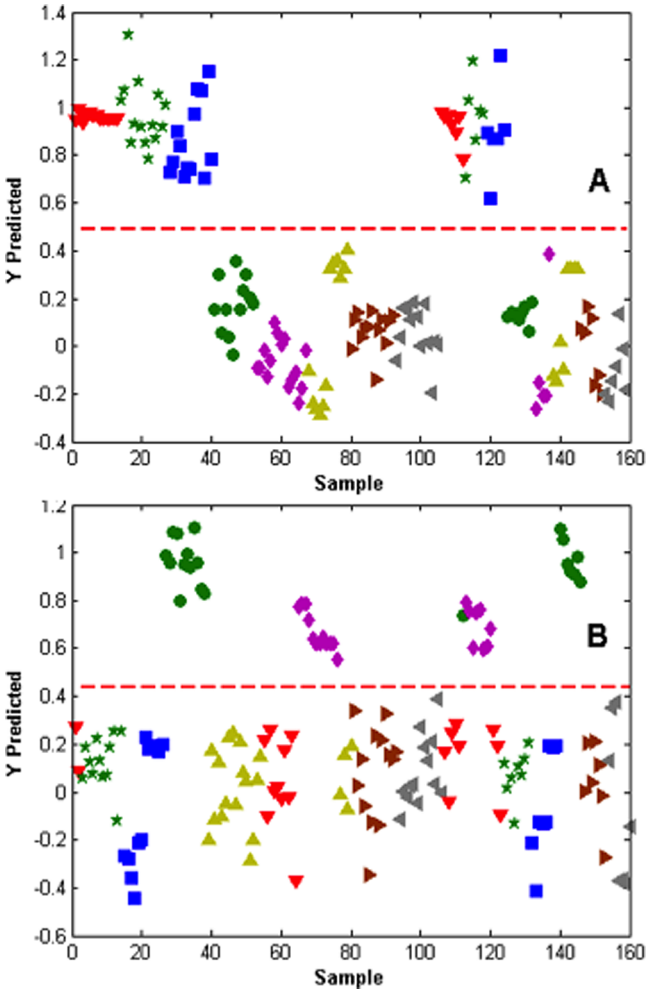

Figure 2. PLS-DA prediction plots for (A) high and (B) low virulence assays. Each colored symbol represents the PLS predicted value for an individual SERS spectrum after incubation of isolated viral RNA at 37 °C for 2 h with the matching DNA probe. (A) Samples 1−40 represent the calibration sets of SERS spectra containing the high virulence strains, including: WH N66S (red ▼), A/CK/TX167280-04/02 (green ★), and A/MuteSwan/MS451072/06 (blue ■). Samples 41−105 represent the calibration sets of low virulence strains and controls, including WH (green ●), A/CK/PA/13609/93 (pink ◇), WH ΔPB1-F2 (yellow ▲), binding buffer (gray ◀), and DNA probe (brown ▶). Samples 106−124 and 125−160 are the validation sets for the high virulence and low virulence/control samples, respectively. (B) Samples 27−38 and 65−76 repent the predicted PLS-DA classification values for the calibration sets of SERS spectra containing the low virulence strains WH (green ●) and A/CK/PA/13609/93 (pink ◇), while samples 112−120 and 140−146 represent the validation sets used to test this model.

Figure 2A represents the results of a PLS-DA classification model designed to identify high virulence strains. Samples 1−40 in Figure 2A represent the predicted PLS-DA classification values for the training set of SERS spectra containing the high virulence strains, including WH N66S, (red ▼), A/CK/TX167280-04/02 (green ★), and A/Mute Swan/MS451072/06 (blue ■). Samples 41−105 represent the predicted classification values for the training set of LPAIV strains and controls, including LPAIV RNA isolated from strains WH (green ●), A/CK/PA/13609/93 (pink ◇), and WH ΔPB1-F2 (yellow ▲); controls included the buffer (gray ◀) and the DNA HPAIV capture probe alone (brown ▶). It is clear from Figure 2A that this method unambiguously separates the spectra of the high and low virulence strains in the calibration sets with complete accuracy.

This high virulence classification model was tested using samples 106−124 and 125−160, which were the validation sets for the high virulence and low virulence/control samples, respectively. Figure 2A qualitatively indicates that this high virulence model accurately classified both low and high virulence validation sets; Table 1 provides the quantitative values. The results show 100% calculated sensitivities and specificities, with root-mean square error of prediction (RMSEP) values of 0.21 for both classes. The overall percentage of test samples correctly classified by the high virulence PLS-DA model was 100%.

Table 1. PLS-DA Results for the Low and High Virulence Determinant Assays

	low virulence		high virulence	
	full hybridization	partial/no hybridization	full hybridization	partial/no hybridization
sensitivity (prediction)	1.00	1.00	1.00	1.00
specificity (prediction)	1.00	1.00	1.00	1.00
RMSEP[a]	0.22	0.22	0.21	0.21
overall % CC[b]	100%		100%	

[a]RMSEP = root-mean-square error of prediction from PLS-DA = $\{(\sum_{i=1}^{n}(\hat{y}_i - y_i)^2)/n\}^{1/2}$, where $\hat{y}_i$ is the predicted value from PLS-DA and y_i is the measured class value. [b]% CC = percent of samples correctly classified = (TP + TN)/(TP + TN + FP + FN), where TP = true positive, TN = true negative, FP = false positive, FN = false negative.

Figure 2B represents the complementary situation for a classification model designed to identify low virulence strains. In similar fashion to Figure 2A, samples 27−38 and 65−76 in Figure 2B represent the predicted PLS-DA classification values for the calibration sets of SERS spectra containing the low virulence strains WH (green ●) and A/CK/PA/13609/93 (pink ◇), while samples 112−120 and 140−146 represent the validation sets used to test this model. Similar to the high virulence model in Figure 2A, the low virulence model in

dx.doi.org/10.1021/ac500659f | Anal. Chem. 2014, 86, 6911−6917

Figure 2B indicates high classification accuracy. Table 1 provides the quantitative results for the low virulence model: calculated sensitivities and specificities of 100% and RMSEP of 0.22, with an overall percentage of correctly classified test samples of 100%. Results from the PLS-DA models show extremely high sensitivities, specificities, and percent correct classification, albeit with relatively high values for RMSEP.

While PLS-DA is a powerful tool for classification and regression, it is not optimized for use with complex, nonlinear data sets.[45,46] Support vector machine-discriminant analysis (SVM-DA) is a relatively new classification and regression method that can produce a unique, global solution when presented with high-dimensional inputs.[47,48] We applied SVM for classification of the high and low virulence strains described above.

For SVM-DA analysis, a radial basis function (RBF) kernel was used and the SVM model was calculated by grid searching within a range of paired values of cost (C = penalty error) and radial width (γ). In this formulation, SVM required fitting two parameters for optimization. The first is γ, defined as $\gamma = 1/(2\sigma^2)$, where σ is the radial width of the RBF that determines the shape of the hyperplane that best separates the different classes. The second parameter C takes into account the regression errors of the training set and controls the complexities of the class boundaries. Once the optimal parameters were determined for the calibration set, the test set was loaded and class membership probabilities calculated using the established SVM-DA calibration model.

The SVM-DA model structure in terms of calibration and validation sets was identical to that described for PLS-DA (see above). The calibration set was first compressed by choosing an optimized rank of latent variables as determined from a cross-validated principal least-squares (PLS) calculation. The optimal pair of SVM parameters (C, γ) was chosen by cross validation (Venetian blinds, 5 splits) of the calibration set. The values used were $\gamma = 100$ and $C = 0.316$ for the high virulence assay and $\gamma = 100$ and $C = 0.001$ for the low virulence assay. A total of 19 support vectors were used in the calculations for both assays.

Figure 3 illustrates the results from the SVM-DA calculations for a high virulence classification model. As in the case of the PLS-DA model (Figure 2A), samples 1−40 represent the training set of SERS spectra containing the HPAIV strains, samples 41−105 represent the training set of low virulence strains and controls, while samples 106−124 and 125−160 are the test sets for the high virulence and low virulence/control samples, respectively. The ordinate axis in Figure 3 is the predicted class membership probability, as calculated by the SVM-DA model. In a binary classification model, the closer the class predicted probability is to 0.0 or 1.0, the more likely the sample is to belong to that particular class. Figure 3A shows that SVM fully separates the high virulence test samples from the low virulence and control samples. Table 2 quantifies the results: the SVM model provides 100% specificity and sensitivity for prediction with 100% of test samples correctly classified. In addition, the SVM model has a root-mean-square error of class predicted probability (RMSECPP) of 0.07, showing a much lower prediction error compare to PLS-DA model, which had an RMSEP value of 0.21.

A similar situation occurs for the low virulence assay illustrated in Figure 3B, in which samples 27−38 and 65−76 represent the predicted SVM class membership probabilities for the calibration sets of SERS spectra containing the low

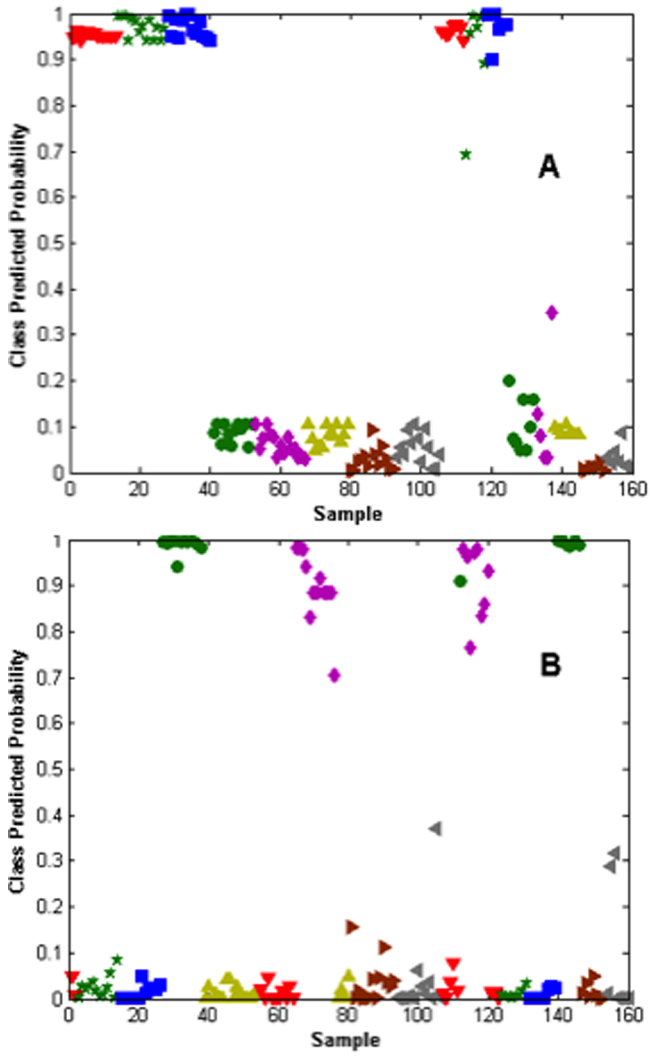

Figure 3. SVM-DA probability plots for (A) high and (B) low virulence assays. Each colored symbol represents the SVM predicted class membership probability for an individual SERS spectrum after incubation of isolated viral RNA at 37 °C for 2 h with the matching DNA probe. The codes for each colored symbol and sample number are WH N66S (red ▼), A/CK/TX167280-04/02 (green ★), and A/MuteSwan/MS451072/06 (blue ■). Samples 41−105 represent the calibration sets of low virulence strains and controls, including WH (green ●), A/CK/PA/13609/93 (pink ◇), WH ΔPB1-F2 (yellow ▲), binding buffer (gray ◀), and DNA probe (brown ▶).

virulence strains WH and A/CK/PA/13609/93, while samples 112−120 and 140−146 represent the validation sets used to test this model. Table 2 provides the quantitative results: the SVM low virulence model showed 100% sensitivity and specificity for prediction with 100% of the test samples correctly classified. The SVM model also had a RMSECPP of 0.06, compared with the prediction errors associated with PLS-DA, i.e., an RMSEP value of 0.22.

■ CONCLUSIONS

We report here the first use of oligonucleotide-modified substrates as diagnostic tools for the direct identification of a PB1-F2 mutation in the influenza virus genome related to virulence, specifically the N66S gene mutation within the PB1-F2 protein. The method employed 5′-thiol-modified ssDNA sequences as probes to capture RNA isolated from avian and

dx.doi.org/10.1021/ac500659f | Anal. Chem. 2014, 86, 6911−6917

Table 2. SVM-DA Results for the Low and High Virulence Determinant Assays

	low virulence		high virulence	
	full hybridization	partial/no hybridization	full hybridization	partial/no hybridization
sensitivity (prediction)	1.00	1.00	1.00	1.00
specificity (prediction)	1.00	1.00	1.00	1.00
RMSECPP[a]	0.06	0.06	0.07	0.07
overall % CC[b]	100%		100%	

[a]RMSECPP = root-mean-square error of class predicted probability from SVM-DA = $\{(\sum_{i=1}^{n}(\hat{CP}_i - CP_i)^2)/_n\}^{1/2}$, where $\hat{CP}_i$ is the predicted value from SVM-DA, and CP_i is the measured class value. [b]% CC = percent of samples correctly classified = (TP + TN)/(TP + TN + FP + FN), where TP = true positive, TN = true negative, FP = false positive, FN = false negative..

reverse genetics influenza viruses containing low virulence or high virulence determinants. We used a label-free and amplification-free optical read-out method, i.e., Raman spectroscopy, to determine the efficacy of binding. The Raman spectra of both high virulence and low virulence DNA-RNA target complexes showed high similarity; therefore, multivariate analysis was used to identify target binding. Binary classification models were developed to distinguish complementary from noncomplementary DNA-RNA target hybrids. The SVM-DA model that was developed using a radial basis function kernel resulted in calculated values of 100% sensitivity, 100% specificity, and 100% correct classification of the test samples with a small root-mean-square error of prediction (RMSECPP ~0.07).

The current study was designed to demonstrate the ability of the SERS methodology to identify different virulence genotypes from real RNA virus-containing specimens, not to determine a lower limit of detection of the assay. However, a previous study using the same ssDNA PB1-F2 probes employed in this article demonstrated that these SERS-based methods were an order of magnitude more sensitive than ELISA for the capture of synthetic influenza RNA target sequences (10 nM vs 100 nM).[30] Also, in terms of the use of these methods for complex biological samples, we have previously shown that the SERS methods described in this paper were simultaneously able to identify eight human rotavirus strains and classify each according to its G or P genotype with >96% accuracy.[49] Other studies showed that our SERS-based methods had equivalent-or-better detection limits than qPCR for analysis of pathogens in complex clinical samples.[50] Therefore, based on our previous experience, we feel confident that the methods described here can be extended to analyze biologically complex mixtures.

These studies establish that optical-based Raman diagnostic methods are able to sensitively and accurately detect influenza virus RNA mutations linked to pathogenicity in emerging highly pathogenic avian and pandemic influenza viruses without amplification or labeling. The results are also the first demonstration of the use of real influenza viral RNA for direct identification of diagnostic indicators of influenza virulence. Future work will address the applicability and robustness of this platform for more relevant samples containing the target viral RNA in complex influenza isolates.

■ ASSOCIATED CONTENT

Supporting Information

Table of virus titer and PFU per 0.2 mL for each of the influenza virus strains used in these experiments (Table S.1). This material is available free of charge via the Internet at http://pubs.acs.org.

■ AUTHOR INFORMATION

Corresponding Author

*E-mail: dluhy@uga.edu. Phone: +1-706-542-1950. Fax: +1-706-542-9454.

Notes

The authors declare no competing financial interest.

■ ACKNOWLEDGMENTS

We thank Dr. Peter Palese (Icahn School of Medicine at Mount Sinai, New York, NY) for providing WH, WH N66S, and WH ΔPB1-F2 viruses used in these studies. This research project was supported by the U.S. Public Health Service through Grant GM102546 from the National Institutes of Health. We would also like to acknowledge funding for the Center of Excellence for Influenza Research and Surveillance (CEIRS; Grant HHSN26620070000C)

■ REFERENCES

(1) WHO. 2013; http://www.who.int/mediacentre/factsheets/fs211/en/index.html.
(2) WHO. 2013; http://www.who.int/influenza/human_animal_interface/H5N1_cumulative_table_archives/en/.
(3) de Jong, M. D.; Simmons, C. P.; Thanh, T. T.; Hien, V. M.; Smith, G. J. D.; Chau, T. N. B.; Hoang, D. M.; Chau, N. V. V; Khanh, T. H.; Dong, V. C.; Qui, P. T.; Van Cam, B.; Ha, D. Q.; Guan, Y.; Peiris, J. S. M.; Chinh, N. T.; Hien, T. T.; Farrar. *J. Nat. Med.* **2006**, *12*, 1203−1207.
(4) Stevens, J.; Blixt, O.; Tumpey, T. M.; Taubenberger, J. K.; Paulson, J. C.; Wilson, I. A. *Science* **2006**, *312*, 404−410.
(5) Muramoto, Y.; Le, T. Q. M.; Phuong, L. S.; Nguyen, T.; Nguyen, T. H.; Sakai-Tagawa, Y.; Horimoto, T.; Kida, H.; Kawaoka, Y. *J. Vet. Med. Sci.* **2006**, *68*, 735−737.
(6) Muramoto, Y.; Le, T. Q. M.; Phuong, L. S.; Nguyen, T.; Nguyen, T. H.; Sakai-Tagawa, Y.; Iwatsuki-Horimoto, K.; Horimoto, T.; Kida, H.; Kawaoka, Y. *J. Vet. Med. Sci.* **2006**, *68*, 527−531.
(7) McAuley, J. L.; Chipuk, J. E.; Boyd, K. L.; Van De Velde, N.; Green, D. R.; McCullers, J. A. *PLoS Pathog.* **2010**, *6*, 1−12.
(8) Solbak, S. M. O.; Sharma, A.; Bruns, K.; Roder, R.; Mitzner, D.; Hahn, F.; Niebert, R.; Vedeler, A.; Henklein, P.; Henklein, P.; Schubert, U.; Wray, V.; Fossen, T. *Biochim. Biophys. Acta* **2012**, *1834*, 568−582.
(9) Smith, A. M.; McCullers, J. A. *Virus Res.* **2013**, *178*, 146−150.
(10) Takahashi, T.; Takaguchi, M.; Kawakami, T.; Suzuki, T. *PLoS One* **2013**, *8*, 1−8.
(11) Conenello, G. M.; Zamarin, D.; Perrone, L. A.; Tumpey, T.; Palese, P. *PLoS Pathog.* **2007**, *3*, 1414−1421.
(12) Krumbholz, A.; Philipps, A.; Oehring, H.; Schwarzer, K.; Eitner, A.; Wutzler, P.; Zell, R. *Med. Microbiol. Immunol.* **2011**, *200*, 69−75.
(13) Pasricha, G.; Mishra, A. C.; Chakrabarti, A. K. *Influenza Other Respir. Viruses* **2013**, *7*, 497−505.
(14) Kash, J. C.; Tumpey, T. M.; Proll, S. C.; Carter, V.; Perwitasari, O.; Thomas, M. J.; Basler, C. F.; Palese, P.; Taubenberger, J. K.; Garcia-Sastre, A.; Swayne, D. E.; Katze, M. G. *Nature* **2006**, *443*, 578−581.
(15) Salomon, R.; Franks, J.; Govorkova, E. A.; Ilyushina, N. A.; Yen, H. L.; Hulse-Post, D. J.; Humberd, J.; Trichet, M.; Rehg, J. E.; Webby, R. J.; Webster, R. G.; Mann, E. H. *J. Exp. Med.* **2006**, *203*, 689−697.
(16) Li, M.; Brenwald, N.; Bonigal, S.; Chana, K.; Osman, H.; Oppenheim, B. *J. Infect.* **2012**, *65*, 60−63.

(17) Driskell, J. D.; Seto, A. G.; Jones, L. P.; Jokela, S.; Dluhy, R. A.; Zhao, Y.-P.; Tripp, R. A. *Biosens. Bioelectron.* **2008**, *24*, 923−928.
(18) Driskell, J.; Primera-Pedorozo, O.; Dluhy, R. A.; Zhao, Y.-P.; Tripp, R. A. *Appl. Spectrosc.* **2009**, *63*, 1107−1114.
(19) Driskell, J. D.; Tripp, R. A. *Chem. Commun.* **2010**, *46*, 3298−3300.
(20) Negri, P.; Kage, A.; Nitsche, A.; Naumann, D.; Dluhy, R. A. *Chem. Commun.* **2011**, *47*, 8635−8637.
(21) Abell, J. L.; Garren, J. M.; Driskell, J. D.; Tripp, R. A.; Zhao, Y. *J. Am. Chem. Soc.* **2012**, *134*, 12889−12892.
(22) Negri, P.; Chen, G.; Kage, A.; Nitsche, A.; Naumann, D.; Xu, B.; Dluhy, R. A. *Anal. Chem.* **2012**, *84*, 5501−5508.
(23) Barhoumi, A.; Zhang, D.; Halas, N. J. *J. Am. Chem. Soc.* **2008**, *130*, 14040−14041.
(24) Barhoumi, A.; Zhang, D.; Tam, F.; Halas, N. J. *J. Am. Chem. Soc.* **2008**, *130*, 5523−5529.
(25) Harpster, M. H.; Zhang, H.; Sankara-Warrier, A. K.; Ray, B. H.; Ward, T. R.; Kollmar, J. P.; Carron, K. T.; Mecham, J. O.; Corcoran, R. C.; Wilson, W. C. *Biosens. Bioelectron.* **2009**, *25*, 674−681.
(26) Sun, L.; Irudayaraj, J. *Biophys. J.* **2009**, *96*, 4709−4716.
(27) Miljanic, S.; Dijanosic, A.; Piantanida, I.; Meic, Z.; Albelda, M. T.; Sornosa-Ten, A.; Garcia-Espana, E. *Analyst* **2011**, *136*, 3185−3193.
(28) Miljanic, S.; Dijanosic, A.; Landeka, K.; Stojkovic, M. R.; Piantanida, I. *Appl. Spectrosc.* **2012**, *66*, 82−89.
(29) Xie, W.; Schlucker, S. *Phys. Chem. Chem. Phys.* **2013**, *15*, 5329−5344.
(30) Negri, P.; Dluhy, R. A. *Analyst* **2013**, *138*, 4877−4884.
(31) Chaney, S. B.; Shanmukh, S.; Zhao, Y.-P.; Dluhy, R. A. *Appl. Phys. Lett.* **2005**, *87*, 31908−31910.
(32) Driskell, J. D.; Shanmukh, S.; Liu, Y.; Chaney, S. B.; Tang, X. J.; Zhao, Y. P.; Dluhy, R. A. *J. Phys. Chem. C* **2008**, *112*, 895−901.
(33) Abell, J. L.; Driskell, J. D.; Dluhy, R. A.; Tripp, R. A.; Zhao, Y. P. *Biosens. Bioelectron.* **2009**, *24*, 3663−3670.
(34) Mundt, E.; Gay, L.; Jones, L.; Saavedra, G.; Tompkins, S. M.; Tripp, R. A. *Arch. Virol.* **2009**, *154*, 1241−1248.
(35) Chen, W.; Calvo, P. A.; Malide, D.; Gibbs, J.; Schubert, U.; Bacik, I.; Basta, S.; O'Neill, R.; Schickli, J.; Palese, P.; Henklein, P.; Bennink, J. R.; Yewdell, J. W. *Nat. Med.* **2001**, *7*, 1306−1312.
(36) Mooney, A. J.; Li, Z.; Gabbard, J. D.; He, B.; Tompkins, S. M. *J. Virol* **2013**, *87*, 363−371.
(37) Brereton, R. G. *Chemometrics for Pattern Recognition*; J. Wiley & Sons, Ltd.: Chichester, U.K., 2009.
(38) Barker, M.; Rayens, W. *J. Chemom.* **2003**, *17*, 166−173.
(39) Xu, Y.; Zomer, S.; Brereton, R. G. *Crit. Rev. Anal. Chem.* **2006**, *36*, 177−188.
(40) Brereton, R. G.; Lloyd, G. R. *Analyst* **2010**, *135*, 230−267.
(41) Maquelin, K.; Kirschner, C.; Choo-Smith, L. P.; Ngo-Thi, N. A.; van Vreeswijk, T.; Stammler, M.; Endtz, H. P.; Bruining, H. A.; Naumann, D.; Puppels, G. J. *J. Clin. Microbiol.* **2003**, *41*, 324−329.
(42) Jarvis, R. M.; Goodacre, R. *Anal. Chem.* **2004**, *76*, 40−47.
(43) Negri, P.; Dluhy, R. A. *J. Biophoton.* **2013**, *6*, 20−35.
(44) Bylesjö, M.; Rantalainen, M.; Cloarec, O.; Nicholson, J. K.; Holmes, E.; Trygg, J. *J. Chemom.* **2006**, *20*, 341−351.
(45) Despagne, F.; Massart, D. L.; Chabot, P. *Anal. Chem.* **2000**, *72*, 1657−1665.
(46) Centner, V.; Verdu-Andres, J.; Walczak, B.; Jouan-Rimbaud, D.; Despagne, F.; Pasti, L.; Massart, D.-L.; Noord, O. E. D. *Appl. Spectrosc.* **2000**, *54*, 608−623.
(47) Thissen, U.; Pepers, M.; Üstün, B.; Melssen, W. J.; Buydens, L. M. C. *Chemom. Intell. Lab. Syst.* **2004**, *73*, 169−179.
(48) Thissen, U.; Üstün, B.; Melssen, W. J.; Buydens, L. M. C. *Anal. Chem.* **2004**, *76*, 3099−3105.
(49) Driskell, J. D.; Zhu, Y.; Kirkwood, C.; Zhao, Y.-P.; Dluhy, R. A.; Tripp, R. A. *PLoS One* **2010**, *5*, e10222.
(50) Hennigan, S. L.; Driskell, J. D.; Ferguson-Noel, N.; Dluhy, R. A.; Zhao, Y.; Tripp, R. A.; Krause, D. C. *Appl. Environ. Microbiol.* **2012**, *78*, 1930−1935.